agricultural engineering.eu 80(3), 2025, 177–188

DOI:10.15150/ae.2025.3337

agricultural engineering.eu

Two-dimensional Crop Flow Separation Model for Rotor Units of Combine Harvesters

Marvin Barther

Today, one-dimensional separation model approaches have been used successfully to estimate the separation efficiency for straw walkers and sieve-based cleaning units. In contrast to straw walkers, estimating the separation efficiency of rotor units with sensors is challenging, because straw and grain are transported along helical trajectories and sensors can only measure a small fraction of the separated grain. This study introduces a novel two-dimensional crop flow separation model based on Böttinger's separation model and Wacker's crop flow model for rotor units. Utilizing a large grid aligned sensor network of structure-borne noise sensors within the combine harvester's rotor unit, the two-dimensional separation model approach fits well on grain masses within single rotor segments. It can be applied straightforwardly to different rotor unit designs and sensor positions.

Keywords

Separation process, combine harvester, crop flow, rotor unit, two-dimensional model

Combine harvesters have a separation unit and a cleaning unit for grain harvesting. The most common approaches for separation units utilize either straw walkers or a rotor unit. The separation efficiency, defined as the amount of grain separated from material other than grain (MOG), is a crucial metric for separation units of combine harvesters (Miu 2015). Commonly, structure-borne noise sensors have been used for grain counting, especially piezoelectric and acoustic sensors (Meyer zu Hoberge and Hilleringmann 2011, Penner et al. 2024).

First approaches towards grain loss predictions based on sensor data used exponential functions to describe the decaying behavior of grain separation along the separation length (Beck 1999, Bjork 1991, Böttinger 1993, Nath et al. 1982). Soon after, the exponential models and the sensor systems were further developed, and the models were fitted on multiple sensors installed under the separation unit (Liu 1990, Liu and Leonard 1993). Additionally, multidimensional models have been designed to include the separation width (Bjork 1991).

For machine automation, especially with machine learning, it became more common to include the raw grain loss sensor signal into the combine optimization algorithms directly or to design virtual grain loss monitors based on combine settings alone (Bomoi et al. 2023, Gundoshmian et al. 2020, Hermann et al. 2016). Additionally, different machine learning algorithms have been evaluated to predict separation efficiency based on a grid-aligned sensor network and machine settings (Penner et al. 2024).

received 28 January 2025 | accepted 13 June 2025| published 10 July 2025

In this study, a novel two-dimensional crop flow separation model is introduced and analyzed. It combines Böttinger's approach of exponential decay of separation processes (Böttinger 1993) with the helical transport trajectories described by Wacker (Wacker 1985).

Approaches by Böttinger and Wacker

Wessel (1968) defined different process steps of the grain in separation processes of sieves, which are shown in Figure 1. The first process step is the segregation between grain and MOG, where grain accumulates towards the sieve, followed by the statistical selection. The grain is finally separated by passing the sieve openings.

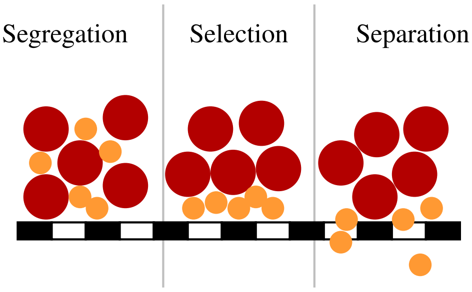

Figure 1: Three parallel process steps for grain according to Wessel (1968): segregation between grain and MOG, selection of grain at the sieves, and separation of grain

Based on the differentiation between segregation and selection, Böttinger (1993) assumed an exponential behavior for both processes, resulting in an inhomogeneous differential equation. A homogeneous grain distribution within the material was assumed as the initial condition. Let A be the coefficient of the segregation process and B that of the selection process, respectively, and let D be a polynomial coefficient. The residual grain functions $\tilde{R}_A(s)$ and $\tilde{R}_B(s)$ describe the amount of not yet separated grain at separation length s for each process, and the residual grain function $\tilde{R}(s) = \tilde{R}_A(s) + \tilde{R}_B(s)$ for the whole process, respectively:

$$\tilde{R}_A(s) = e^{-\frac{A}{D+1}s^{D+1}} \quad \text{(Eq. 1)}$$

$$\tilde{R}_B(s) = \frac{A}{B-A}\left(e^{-\frac{A}{D+1}s^{D+1}} - e^{-\frac{B}{D+1}s^{D+1}}\right) \quad \text{(Eq. 2)}$$

$$\tilde{R}(s) = \frac{1}{B-A}\left(Be^{-\frac{A}{D+1}s^{D+1}} - Ae^{-\frac{B}{D+1}s^{D+1}}\right) \quad \text{(Eq. 3)}$$

The separation function $\tilde{Z}(s)$ describes the grain separation rate at separation length s. It is the derivative of the sum of separated grain, which can be described as $1 - \tilde{R}(s)$ with respect to the separation length s:

$$\tilde{Z}(s) = \frac{\partial\left(1 - \tilde{R}(s)\right)}{\partial s} = \frac{AB^2}{B-A}s^D\left(e^{-\frac{A}{D+1}s^{D+1}} - e^{-\frac{B}{D+1}s^{D+1}}\right) = Bs^D \cdot \tilde{R}_B(s) \quad \text{(Eq. 4)}$$

WACKER (1985) described the material trajectory movement inside the rotor unit. The rotor casing can be split into a rotor concave area and a roof panel area, which differ in separation process activation and rearward material thrust. The rotor concave area has sieves and grain can be separated. Typically, the concave area constitutes the lower half of the rotor casing, separating the grain directly onto the return pan underneath the rotor unit. Due to the rotor movement, the material movement is forced to be nearly orthogonal to the combine's length. The roof panel area is closed. The grain can be segregated, but there is no separation. The material gets its rearward thrust by the guide plates in the roof panel area. In Figure 2, the cylindrical rotor casing has been unwrapped into a plane with length x and rotor circumference (plane width) y. Finally, the material is transported in the axial direction through the rotor unit, following a helical trajectory. With each circulation, it is alternately transported through both the concave and roof panel area. Figure 2 illustrates an exemplary crop flow with four circulations.

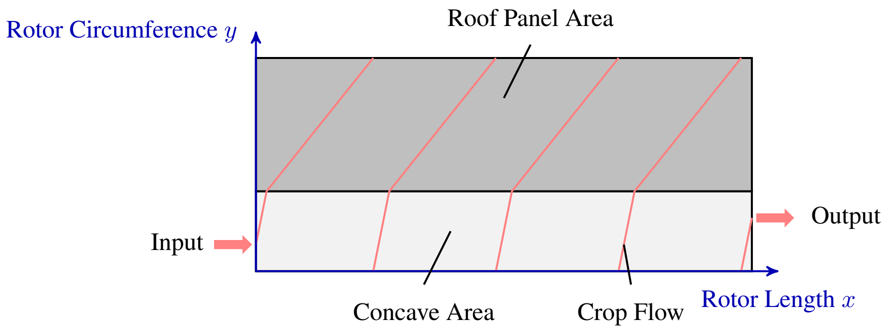

Figure 2: Opened rotor casing defined by Wacker (1985) as a plane with rotor length x and rotor circumference y (For a better overview, the start of the rotor circumference is at the very beginning of the concave area. Beyond the end of the roof panel area, the rotor circumference extends into the concave area. The red line indicates an exemplary crop flow. Due to the periodical rotor circumference, it is alternately transported through the concave and roof panel areas. In this rotor unit, the material undergoes four complete circulations. The material is fed across the rotor circumference, with its trajectories running parallel to the illustrated crop flow example.)

Two-dimensional Crop Flow Separation Model Design

Following the material flow shown in Figure 2, the rotor areas change. Due to the ongoing segregation process in all areas, the homogeneous distribution of grain in the material at the beginning of a rotor concave area can no longer be used as an initial condition. In this study, grain distribution values [0,1] and $\alpha_B \in [0,1]$ with $\alpha_A + \alpha_B = 1$ are introduced as start values at s_0 or both processes, respectively. The residual grain function including the starting value of the segregation process $\check{R}_A(s)$ can be adapted from equation 1:

$$\check{R}_A(s) = \alpha_A e^{-\frac{A}{D+1}s^{D+1}} \quad \text{(Eq. 5)}$$

The starting value for the residual grain function of the selection process $\check{R}_A(s)$ must be included in the solution of Böttinger's inhomogeneous differential equation (BÖTTINGER 1993):

$$\check{R}_B(s) = e^{-\frac{B}{D+1}s^{D+1}} \cdot \left[\alpha_B + \int_0^s \alpha_A A s^D e^{-\frac{A}{D+1}x^{D+1}} \cdot e^{\frac{B}{D+1}x^{D+1}} \,\mathrm{d}x\right] \quad \text{(Eq. 6)}$$

Finally, the residual functions $\check{R}_B(s)$ and $\check{R}_A(s)$, as well as the separation function $\check{Z}(s)$ can be calculated the same way as $\check{R}_B(s)$, $\check{R}_A(s)$, and $\check{Z}(s)$ (equations 2 to 4):

$$\check{R}_B(s) = \alpha_B e^{-\frac{B}{D+1}s^{D+1}} + \alpha_A \frac{A}{B-A}\left(e^{-\frac{A}{D+1}s^{D+1}} - e^{-\frac{B}{D+1}s^{D+1}}\right) \quad \text{(Eq. 7)}$$

$$\check{R}(s) = \alpha_B e^{-\frac{B}{D+1}s^{D+1}} + \alpha_A \frac{1}{B-A}\left(Be^{-\frac{A}{D+1}s^{D+1}} - Ae^{-\frac{B}{D+1}s^{D+1}}\right) \quad \text{(Eq. 8)}$$

$$\check{Z}(s) = \alpha_B Bs^D e^{-\frac{B}{D+1}s^{D+1}} + \alpha_A \frac{AB}{B-A}s^D\left(e^{-\frac{A}{D+1}s^{D+1}} - e^{-\frac{B}{D+1}s^{D+1}}\right) \quad \text{(Eq. 9)}$$

While $\check{Z}(s)$ (equation 4) always starts at $\check{Z}(s_0)$ and reaches a maximum, $\check{Z}(s)$ (equation 9) can be a single exponential function, strictly monotonically decreasing, with $\alpha_A = 0$.

In Figure 3(a) the activation and deactivation of both the segregation and the selection process are shown along the separation length. By integrating over the separation length s, there are two different process lengths for segregation and selection, which are shown in Figure 3(b).

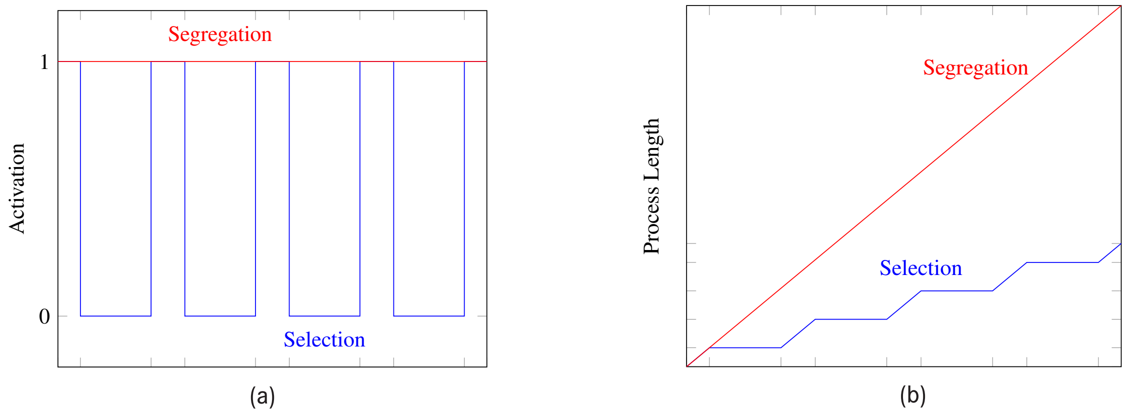

Figure 3: Activation functions of the processes segregation and selection with 1 for activation and 0 for deactivation in (a) and their integrated process lengths in (b) based on the crop flow of Figure 2.

While the segregation length increases linearly, the selection length increases the same way only in rotor concave areas. The selection length remains constant in the roof panel areas. In contrast to the activation function of the selection in Figure 3(a), the selection length function is continuous. This motivates a crop flow separation model approach of a continuous function of sums of single separation functions over all areas. In each area, the specific continuous length functions for segregation and selection are considered.

With given coordinates x and y for the rotor casing length and width, respectively (Figure 2), the material path can be described as an order of different areas with specific selection lengths and selection activations. Let p_i be the upper boundary of area i with $p_i < p_{i+1}$ and $p_0 = 0$. Let $a_i \in \{0,1\}$ be the selection activation of area i. Let n be the corresponding area of separation length s. The selection length s_B is the sum of all active segments of the area:

$$s_B = (s - p_{n-1}) \cdot a_n + \sum_{i=1}^{n-1} (p_i - p_{i-1}) \cdot a_i \qquad \text{(Eq. 10)}$$

With the residual separation length function $q(i)$, the separation length from area i to s (with index k denoting rotor panel area with respective bounds p_{k-1} and p_k and selection activation a_k) can be calculated as follows:

$$q(i) = (s - p_{n-1}) \cdot a_n + \sum_{k=i}^{n-1} (p_k - p_{k-1}) \cdot a_k \qquad \text{(Eq. 11)}$$

While the residual grain function of the segregation process $R_A(s)$ is the same as $\check{R}_A(s)$ (equation 5), the integral of equation 6 must be solved separately for each area i for $R_B(s)$. The area i is integrated only over its length from zero to $p_i – p_{i-1}$. For both the segregation process and the selection process, the already processed length must be considered. While the segregation is continuous, for the selection process the activation a_i must be considered with its already processed length $s_B – q(i)$. All in all, the residual grain function of the selection $R_B(s)$ must be calculated in the following way:

$$R_B(s) = \alpha_B e^{-\frac{B}{D+1} s_B^{D+1}} + e^{-\frac{B}{D+1} s_B^{D+1}} \sum_{i=1}^{n} R_{B,i}(s) \qquad \text{(Eq. 12)}$$

The residual grain function $R_{B,i}(s)$ is the single residual grain function of the selection for area i. With $p_s = min_{(pi,s)}$, its integral (analog to formula 6) must be solved as follows:

$$R_{B,i}(s) = \int_0^{p_s - p_{i-1}} \alpha_A A (x + p_{i-1})^D e^{-\frac{A}{D+1}(x + p_{i-1})^{D+1}} \cdot e^{\frac{B}{D+1}\left(x a_i + s_B - q(i)\right)^{D+1}} \, \mathrm{d}x \qquad \text{(Eq. 13)}$$

In general, the integral in formula 13 has no analytical antiderivative for arbitrary polynomial factors D. The calculation of the two-dimensional crop flow separation model will be continued with $D = 0$ based on Böttinger's approach with the assumption $A \neq B$:

$$R_{B,i}(s) = \int_0^{p_s - p_{i-1}} \alpha_A A e^{-A(x + p_{i-1})} \cdot e^{B\left(x a_i + s_B - q(i)\right)} \, \mathrm{d}x \qquad \text{(Eq. 14)}$$

$$= \alpha_A A \frac{e^{-A p_{i-1}} e^{-B q(i)}}{B a_i - A} \left(e^{(B a_i - A)(p_s - p_{i-1})} - 1\right) \qquad \text{(Eq. 15)}$$

The residual grain function $R(s)$ and the separation function $Z(s)$ are calculated the same way as $\check{R}(s)$ and $\check{Z}(s)$ (equations 3 and 4), respectively:

$$R(s) = \alpha_B e^{-B s_B} + \alpha_A \frac{B a_n}{B a_n - A} e^{-A s}$$

$$+ \alpha_A A \sum_{i=1}^{n-1} \left[\frac{e^{-A p_{i-1}} e^{-B q(i)}}{B a_i - A} \left(e^{(B a_i - A)(p_i - p_{i-1})} - 1\right) \right] - \alpha_A A \frac{e^{-A p_{n-1}} e^{-B q(n)}}{B a_n - A} \qquad \text{(Eq. 16)}$$

$$+\alpha_A A B a_n \sum_{i=1}^{n-1}\left[\frac{e^{-Ap_{i-1}}e^{-Bq(i)}}{Ba_i - A}\left(e^{(Ba_i - A)(p_i - p_{i-1})} - 1\right)\right] - \alpha_A A B a_n \frac{e^{-Ap_{n-1}}e^{-Bq(n)}}{Ba_n - A} \qquad \text{(Eq. 17)}$$

The separation function *Z(s)* in equation 17 can also be written as *Z(s)* = B$a_n \cdot R_B(s)$.

Continuity and Differentiability

Both the residual function *R(s)* and the separation function *Z(s)* are sums of exponential functions. Exponential functions are continuously differentiable on the whole domain of $\mathbb{R}$. To check for continuity and differentiability, the boundaries between the exponential functions must be considered. For the residual function *R(s)*, the limits of *s* approaching the boundary point p_n from both sides, from area *n* and from area *n + 1*, must be equal:

$$\lim_{s \nearrow p_n} R(s) = \lim_{s \searrow p_n} R(s) \qquad \text{(Eq. 18)}$$

First, it can be easily proven that the limits of s_B (equation 10) with $s = p_n$ are the same:

$$\lim_{s \searrow p_n} s_B = \sum_{k=1}^{(n+1)-1}\left[(p_k - p_{k-1}) \cdot a_k\right] + (p_n - p_n) \cdot a_{n+1} \qquad \text{(Eq. 19)}$$

$$= \sum_{k=1}^{n}\left[(p_k - p_{k-1}) \cdot a_k\right] \qquad \text{(Eq. 20)}$$

$$= \sum_{k=1}^{n-1}\left[(p_k - p_{k-1}) \cdot a_k\right] + (p_n - p_{n-1}) \cdot a_n = \lim_{s \nearrow p_n} s_B \qquad \text{(Eq. 21)}$$

This proves the equality of the first term $\alpha_B e^{-Bs_B}$ of equation 16. Using equation 11, it can be shown that $q(n + 1) = 0$, while $q(n) = (p_n - p_{n-1}) \cdot a_n$. Approaching p_n from area $n + 1$, the second and last term of equation 16 can be reduced as follows:

$$\lim_{s \searrow p_n} \alpha_A \left(\frac{Ba_{n+1}}{Ba_{n+1} - A} e^{-As} - \frac{Ae^{-Ap_n}e^{-Bq(n+1)}}{Ba_{n+1} - A}\right) = \alpha_A e^{-Ap_n} \qquad \text{(Eq. 22)}$$

Finally, $\lim_{s \searrow p_n} R(s)$ can be written in the following way:

$$\lim_{s \searrow p_n} R(s) = \alpha_B e^{-Bs_B} + \alpha_A e^{-Ap_n} + \alpha_A A \sum_{i=1}^{n}\left[\frac{e^{-Ap_{i-1}}e^{-Bq(i)}}{Ba_i - A}\left(e^{(Ba_i - A)(p_i - p_{i-1})} - 1\right)\right] \qquad \text{(Eq. 23)}$$

Approaching p_n from area n, the second and last term of equation 16 can be restructured as follows:

$$\lim_{s\nearrow p_n} \alpha_A \left(\frac{Ba_n}{Ba_n - A} e^{-As} - \frac{Ae^{-Ap_{n-1}} e^{-Bq(n)}}{Ba_n - A} \right) \quad \text{(Eq. 24)}$$

$$= \alpha_A A \frac{e^{-Ap_n} - e^{-Ap_{n-1}} e^{-Bq(n)}}{Ba_n - A} + \alpha_A e^{-Ap_n} \quad \text{(Eq. 25)}$$

Finally, e^{-Ap_n} can be expanded:

$$e^{-Ap_n} = e^{-Ap_{n-1}} e^{-Bq(n)} e^{(Ba_n - A)(p_n - p_{n-1})} \quad \text{(Eq. 26)}$$

Inserting equation 26 into equation 25 finally yields:

$$\lim_{s\nearrow p_n} \alpha_A \left(\frac{Ba_n}{Ba_n - A} e^{-As} - \frac{Ae^{-Ap_{n-1}} e^{-Bq(n)}}{Ba_n - A} \right)$$
$$= \alpha_A A \frac{e^{-Ap_{n-1}} e^{-Bq(n)}}{Ba_n - A} \left(e^{(Ba_n - A)(p_n - p_{n-1})} - 1 \right) + \alpha_A e^{-Ap_n} \quad \text{(Eq. 27)}$$

The first term of equation 27 has the same form as the formula in the sum of equation 16 for the nth area. This indicates that the sum of equation 16 can be calculated including the n^{th} area. Finally, the formula for $\lim_{s\searrow p_n} R(s)$ is the same as equation 23. With $\lim_{s\searrow p_n} R(s) = \lim_{s\searrow p_n} R(s)$ the continuity of $R(s)$ is proven.

The residual grain function of process A consists of a single exponential function (equation 5), trivially rendering $R_A(s)$ continuously differentiable. The continuity of $R_B(s)$ can be proven the same way as for $R(s)$. Considering $R(s) = R_A(s) + R_B(s)$ with continuous $R(s)$ and $R_A(s)$; $R_B(s)$ must be continuous, too.

With $Z(s) = Ba_n \cdot R_B(s)$, it can be easily shown that the separation function $Z(s)$ is only continuous *in* $s = p_n$ if $a_n = a_{n+1}$. This indicates that the residual grain function $R(s)$ is only differentiable in $s = p_n$ if $a_n = a_{n+1}$.

Integration into Rotor Casing Plane

The residual function $R(s)$ and the separation function $Z(s)$ are integrated into the rotor casing area in a helical way, as shown in Figure 2. The fed material mass flow Q_{in} is uniformly distributed over the rotor circumference at the beginning of the casing plane at $x = 0$. Let $s(x,y)$ be the separation length at position x and y. The residual grain mass flow and the separation mass rate are given by $Q_{in} b^{-1} \cdot R(s(x,y))$ and $Q_{in} b^{-1} \cdot Z(s(x,y))$, respectively, where b denotes the rotor circumference.

In order to calculate the residual grain $G(x)$ at a specific rotor length , the residual grain must be integrated over the entire rotor circumference y of rotor length x:

$$G(x) = \frac{Q_{\text{in}}}{b} \cdot \int_0^b R\big(s(x,y)\big)\,\mathrm{d}y \quad \text{(Eq. 28)}$$

Equation 28 must be solved by numerical integration methods such as the trapezoidal rule or Simpson's rule (Deuflhard 2008). While Q_{in} and b are constant, it has been proven that $R(s)$ is continuous independent of area boundaries. This allows calculating $G(x)$ with equation 28 at any length

$x \in \mathbb{R}$. To get the separated mass flow $M(x_i, x_{i+1})$ in a specific area range between the lengths x_i and x_{i+1}, the difference between the rest grain mass flows at these lengths must be calculated:

$$M(x_i, x_{i+1}) = G(x_i) - G(x_{i+1}) \quad \text{(Eq. 29)}$$

Test-Setup

Multiple test runs with dry wheat and with different rotor settings have been recorded on a rotor test bench (Figure 4), including two market available rotor types with major differences in geometry. The ratio between the concave and roof panel area sizes of rotor type 1 was about 10 % smaller than that of rotor type 2. But the rotor circumference of rotor type 1 was more than 20 % larger than that of the rotor circumference of rotor type 2.

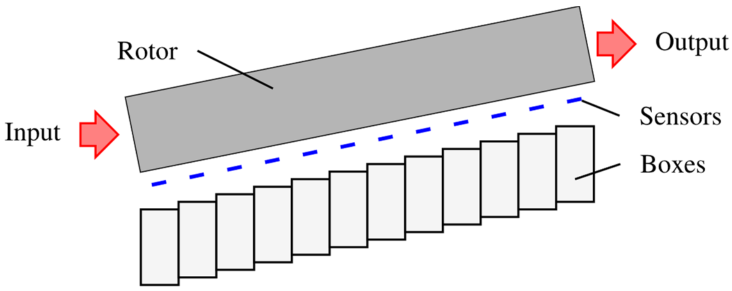

Figure 4: Test Bench Setup with sensors underneath the rotor unit and twelve boxes for collecting grain mass reference.

For the test runs, different throughputs and material compositions of grain and straw have been considered. With each material composition and throughput, the rotor speed has been adjusted in recommended ranges for dry wheat.

A two-dimensional grid-aligned sensor network with structure-borne noise sensors was installed underneath the rotor unit. For reference, twelve boxes for material collection were installed underneath the rotor unit and the sensor network. After each test run, the collected material was cleaned and the grain mass measured. The ratio between measured grain count of the sensor network and the collected reference grain mass was determined for each test run by estimating the mass per thousand grains.

As model references, two different approaches were tested: As a first reference, Bjork's method using exponential functions (Bjork 1991) was tested. For each position at rotor length x, an exponential function $\tilde{Z}_x(y)$ was fitted onto the sensor values along the rotor circumference y. Based on each average sensor value $\bar{\bar{v}}_x$ with

$$\bar{\bar{v}}_x = \frac{1}{b}\int_0^b \tilde{Z}_x(y)\,\mathrm{d}y \quad \text{(Eq. 30)}$$

with rotor circumference size b Böttinger's separation function $\check{Z}(s)$ (equation 9) was fitted to the sensor values along the rotor length x. As a second reference, Böttinger's separation function $\check{Z}(s)$ (equation 9) has been fitted onto a single sensor line at the beginning of the concave area along the rotor length x.

For all reference models, the predicted masses per box $\widetilde{M}(x_i, x_{i+1})$ between the rotor lengths x_i and x_{i+1} are the differences between the residual grain mass flows $\tilde{R}(x_i)$ and $\tilde{R}(x_{i+1})$ (the rotor length x equals the separation length s) simply multiplied by the rotor circumference b:

$$\widetilde{M}(x_i, x_{i+1}) = b \cdot \left(\tilde{R}(x_i) - \tilde{R}(x_{i+1})\right) \qquad \text{(Eq. 31)}$$

Results

The two-dimensional separation model and the reference models were fitted to the sensor values for each test run. Using equations 29 and 31, the grain masses for each box were predicted. In Figure 5, the grain masses of all separation models and the measured grain masses of the boxes of a single test run are shown. The two-dimensional crop flow separation model is qualitatively closest to the ground-truth, whereas the reference models tend to both overestimate and underestimate the grain masses for the first and last boxes, respectively. For the last boxes, all models overestimate the collected grain masses, while the prediction of the two-dimensional crop flow separation model is closest to the reference masses.

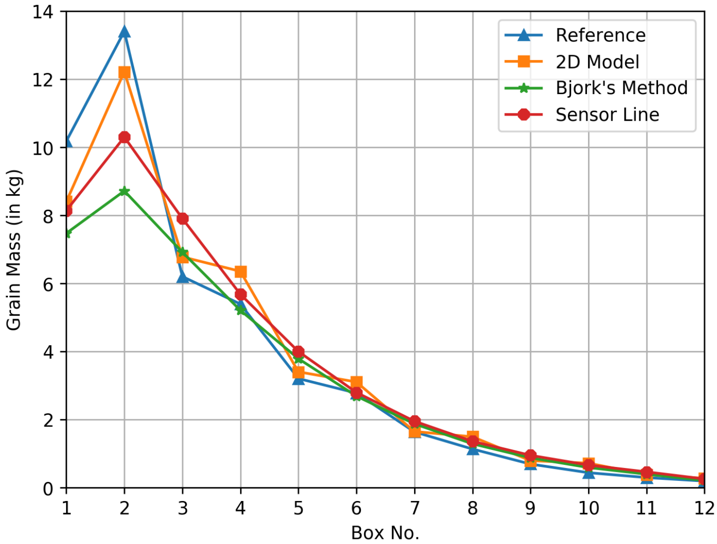

Figure 5: Grain mass estimations of a single test with reference data (collected material in boxes), the predictions of the two-dimensional separation model (2D Model), Bjork's model (Bjork's Method), and Böttinger's model fitted onto a single sensor line (Sensor Line).

For a quantitative comparison, the relative bias between the prediction values $\hat{y}_i$ of the model and the reference data y_i as ground-truth given by the mean signed percentage deviation (MSPD) with

$$\text{MSPD} = \frac{1}{N}\sum_{i=0}^{N}\frac{y_i - \hat{y}_i}{\hat{y}_i} \qquad \text{(Eq. 32)}$$

and the residual deviation by the unbiased root mean squared percentage error (ubRMSPE) with

$$\text{ubRMSPE} = \sqrt{\frac{1}{N}\sum_{i=0}^{N}\left(\frac{y_i - \hat{y}_i}{\hat{y}_i}\right)^2 - \text{MSPD}^2} \qquad \text{(Eq. 33)}$$

were calculated for each test run. A positive and negative bias thus indicate an underestimation and overestimation of the model, respectively (Entekhabi et al. 2009, Hyndman and Koehler 2006). In Table 1, the means and standard deviations of the bias and the residual deviations over all test runs are presented, separately for both tested rotor types.

The most important difference between the two-dimensional crop flow separation model and the reference models is the bias. The mean bias of the two-dimensional crop flow separation model is the best for both rotor types, with one rotor type slightly overestimated and the other one underestimated. While the model for a single sensor line fits with rotor type 2 with the smallest standard deviation for the bias, rotor type 1 was overestimated. Bjork's method shows both underestimation and overestimation. Interestingly, the residual deviation is slightly worse for the two-dimensional crop flow separation model.

Table 1: Results of the two-dimensional crop flow separation model (2D Model) and the reference models, model approach by Bjork (Bjork' Method) and model fits on single sensor line with Böttinger's model (Sensor Line). For the Bias and the residual deviation, both mean and standard deviation (STD) are listed.

Model	Rotortype	Bias Mean	Bias STD	Residual Mean	Residual STD
2D Model	1	-8.37 %	26.79 %	29.13 %	31.09 %
	2	5.18 %	17.46 %	26.95 %	15.31 %
Bjork's Method	1	-17.58 %	20.11 %	20.12 %	11.86 %
	2	17.81 %	10.00 %	24.80 %	6.06 %
Sensor Line	1	-29.04 %	21.85 %	25.13 %	28.09 %
	2	-6.23 %	9.35 %	22.24 %	6.39 %

Discussion

The advantage of the two-dimensional crop flow separation model is the inclusion of the rotor geometry. This leads to the lowest relative mean bias in absolute values in this comparison. Both reference models show both overestimation and underestimation for at least one rotor type. Evidently, the rotor circumference b alone (as in formula 31) is not sufficient for the reference models to predict the grain mass in width of the separation area. A calibration factor, at minimum including the rotor circumference and the ratio between the concave and roof panel areas, must be evaluated.

The residual deviation is slightly worse for the two-dimensional crop flow separation model. With the assumption of normally distributed residual deviation, the models' residual deviations could be reduced by taking the mean over time. A bias correction can only be achieved by calibration, so it is the more important metric, in our case. With its bias closest to zero, the novel two-dimensional crop flow separation model can thus be considered the superior model for rotor units.

Conclusions

In this study, a two-dimensional crop flow separation model for rotor units was proposed, based on Böttinger's separation model for straw walkers and sieve-based cleaning units, as well as the helical transport trajectories of the rotor unit defined by Wacker. The model is designed as a sum of separation models for each area the material is passing through, considering the specific separation behavior of each area. The grain residual functions of the two-dimensional model were shown to be continuous in each point in the separation area. This indicates that the separated grain mass can be calculated for each position.

In a test bench setup, the two-dimensional crop flow separation model was compared to Bjork's model approach, and Böttinger's one-dimensional model. The models were fitted onto a grid-aligned sensor network for grain estimation to predict the separated grain masses of separation sections validated by collected grain material.

While Bjork's method and Böttinger's one-dimensional approach still need calibration factors, the novel two-dimensional crop flow separation model achieved the lowest bias in absolute values. Its advantage is the inclusion of the rotor geometry. This implies further development of the model to become more independent of material characteristics and machine settings. This can be achieved, for example, by a more precise helical transport trajectory description of the material thrust in the rotor unit.

References

Beck, F. (1999): Simulation der Trennprozesse im Mähdrescher. In: Fortschrittberichte VDI, Reihe 14: Landtechnik/ Lebensmitteltechnik Nr. 92, Düsseldorf, VDI Verlag

Bjork, A. (1991): A three-dimensional arithmetic model to calculate grain separation and losses for a rotary combine. Canadian Agricultural Engineering 33(2), pp. 245–253

Bomoi, M. I.; Nawi, N. M.; Aziz, S. A.; Kassim, M. S. M. (2023): Application of Artificial Neural Networks and Genetic Algorithm for the Prediction of Grain Loss from a Medium-sized Combine Harvester. In: Proceedings of the XL CIOSTA and CIGR Section V International Conference, Évora, Portugal, September 10-13

Böttinger, S. (1993): Die Abscheidefunktion von Hordenschüttler und Reinigungsanlage in Mähdreschern. In: Fortschrittberichte VDI, Reihe 14: Landtechnik/Lebensmitteltechnik Nr. 66, Düsseldorf, VDI Verlag

Deuflhard, P.; Hohmann, A. (2008): Numerische Mathematik 1 – Eine algorithmische orientierte Einführung. Berlin, Walter de Gruyter Verlag

Entekhabi, D.; Reichle, R. H.; Koster, R. D.; Crow, W. T. (2010): Performace Metrics for Soil Moisture Retrievals and Application Requirements. Journal of Hydrometeorology 11(3), https://doi.org/10.1175/2010jhm1223.1

Gundoshmian, T. M.; Ardabili, S.; Mosavi, A.; Várkonyi-Kóczy, A. R. (2020): Prediction of Combine Harvester Performance Using Hybrid Machine Learning Modeling and Response Surface Methodology. In: Várkonyi-Kóczy, A. (eds) Engineering for Sustainable Future, INTER-ACADEMIA 2019, Switzerland, Springer Nature Switzerland, pp. 345–360, https://doi.org/10.1007/978-3-030-36841-8_34

Hermann, D.; Bilde, M.; Andersen, N.; Ravn, O. (2016): A framework for semi-automated generation of a virtual combine harvester. IFACPapersOnLine 49(16), pp. 55–60, https://doi.org/10.1016/j.ifacol.2016.10.011

Hyndman, R.J.; Koehler, A. B. (2006): Another look at measures of forecast accuracy. International Journal of Forecasting 22(4), https://doi.org/10.1016/j.ijforecast.2006.03.001

Liu, C. (1990): Microprocessor Based Real-Time Grain Loss Monitoring and Prediction System for an Axial-Flow Combine. Master thesis, Department of Agricultural Engineering, University of Alberta, Edmonton, Alberta, Canada, https://era.library.ualberta.ca/items/0e325e5c-5933-457c-b6bd-42fcd67b4c88, accessed on 10 July 2025

Liu, C.; Leonard, J. (1993): Monitoring actual grain loss from an axial flow combine in real time. Computers and Electronics in Agriculture 9(3), pp. 231–242, https://doi.org/10.1016/0168-1699(93)90041-X

Meyer zu Hoberge, S.; Hilleringmann, U. (2011): Piezoelectric Sensor Array with Evaluation Electronic for Counting Grains in Seed Drills. In: IEEE Africon 2011 - The Falls Resort and Conference Centre. Livingstone, Zambia, September 13–15, https://doi.org/10.1109/AFRCON.2011.6072063

Miu, P. (2015) Combine Harvesters – Theory, Modeling, and Design. Boca Raton, Florida, USA, Taylor & Francis Group, https://doi.org/10.1201/b18852

Nath, S.; Johnson, W. H.; Milliken, G. A. (1982): Combine Loss Model and Optimization of the Machine System. Transactions of the ASAE. 25 (2), https://doi.org/10.13031/2013.33526

Penner, K.; Barther, M.; Wittenfeld, F.; Hesse, M.; Thies, M. (2024): Evaluation of machine learning-driven sensor networks for observing separation processes in combine harvesters for estimating separation efficiency. In: AgEng 2024 Proceedings, Athen, July 01–04, pp. 578–585

Wacker, P. (1985): Untersuchungen zum Dresch- und Trennvorgang von Getreide in einem Axialdreschwerk. Dissertation, Universität Hohenheim

Wessel, J. (1968): Verfahren des Siebens und des Windsichtens. Grundlagen der Landtechnik 18(4), S. 151–157

Author

Marvin Barther M. Sc. is a doctoral student and works at Advanced Development Process Automation, CLAAS Selbstfahrende Erntemaschinen GmbH, Mühlenwinkel 1, 33428 Harsewinkel. E-mail: marvin.barther@claas.com

Acknowledgements

I would like to thank CLAAS for their cooperation and contributions to this work.